Marangoni driven turbulence in high energy surface melting processes

Kidess, Anton; Kenjeres, S.; Righolt, Bernhard W.; Kleijn, Chris R.

DOI
10.1016/j.ijthermalsci.2016.01.015

Publication date
2016

Document Version
Accepted author manuscript

Published in
International Journal of Thermal Sciences

Link to formal publication International Journal of Thermal Sciences (Elsevier): http://dx.doi.org/10.1016/j.ijthermalsci.2016.01.015

Marangoni driven turbulence in high energy surface melting processes

Anton Kidess[a,b,*], Saša Kenjereš[a,b], Bernhard W. Righolt[a,b], Chris R. Kleijn[a,b]

[a] *Department of Chemical Engineering, Delft University of Technology, Julianalaan 136, 2628BL Delft, Netherlands*
[b] *JM Burgers Centre for Fluid Mechanics, Mekelweg 2, 2628CD Delft, Netherlands*

Abstract

Experimental observations of high-energy surface melting processes, such as laser welding, have revealed unsteady, often violent, motion of the free surface of the melt pool. Surprisingly, no similar observations have been reported in numerical simulation studies of such flows. Moreover, the published simulation results fail to predict the post-solidification pool shape without adapting non-physical values for input parameters, suggesting the neglect of significant physics in the models employed. The experimentally observed violent flow surface instabilities, scaling analyses for the occurrence of turbulence in Marangoni driven flows, and the fact that in simulations transport coefficients generally have to be increased by an order of magnitude to match experimentally observed pool shapes, suggest the common assumption of laminar flow in the pool may not hold, and that the flow is actually turbulent. Here, we use direct numerical simulations (DNS) to investigate the role of turbulence in laser melting of a steel alloy with surface active elements. Our results reveal the presence of two competing vortices driven by thermocapillary forces towards a local surface tension maximum. The jet away from this location at the free surface, separating the two vortices, is found to be unstable and highly oscillatory, indeed leading to turbulence-like flow in the pool. The resulting additional heat transport, however, is insufficient to account for the observed differences in pool shapes between experiment and simulations.

Keywords: Marangoni flow, Thermocapillary flow, Turbulence, Direct numerical simulation, Welding

1. Introduction

A long-standing question in the modelling of weld pool hydrodynamics is the one of the possible occurrence of turbulence and its influence on heat and momentum transfer. The underlying problem is that no welding model seems to exhibit true predictive capabilities, not even with respect to such a simple overall weld pool property as its post-solidification shape. Rather, all simulations require the adaptation of unphysical input parameters and/or material properties to truthfully reproduce experimental results. For instance, Winkler et al. [1] and Pavlyk and Dilthey [2] tune the heat input characteristics as well as the concentration of surface active species to obtain results matching experiments. More commonly, many authors (e.g. [2–8]) resort to the modification (i.e. enhancement) of transport coefficients, specifically thermal conductivity and viscosity, to match experimental results. No guideline has been established on how to modify the transport properties and generally they are tuned on an ad-hoc basis without any physical reasoning and a priori dependence on weld pool properties. For example, Pitscheneder et al. [7] enhance the molecular thermal conductivity and dynamic viscosity by a constant factor 7 to match experiments, Anderson et al. [3] increase only the viscosity by a constant factor 30, Mishra et al. [9] increase only the thermal conductivity by a factor 4, De and DebRoy [4] propose an optimization algorithm to determine the best values for thermal conductivity and viscosity with multiplication factors up to 17. Even when uncertainties in boundary conditions, e.g. heat transfer efficiency and energy distribution, are minimal, such as in the conduction-mode (i.e. with negligible vaporization) laser welding experiments conducted by Pitscheneder et al. [7], enhanced transport coefficients are required to match experimental weld shapes, strongly suggesting that the published weld pool models lack the inclusion of significant physics.

Furthermore, previously published computational studies fail to report oscillations and non-axisymmetric flow patterns at the liquid surface, such as have been observed in experiments for conduction-mode laser and autogeneous gas tungsten arc welds. Kraus [10] observes that "weld pool surface temperature profiles do not reach quasi-steady-state conditions, but rather vary around some time-averaged or mean values". Zehr [11] reports that "high speed video images of the melt pool seem to reveal substantial oscillations of the free surface as the laser interacts with the workpiece". Finally, Zhao et al. show highly unstable flow with multiple flow cells using surface particle-image-velocimetry of a gas-tungsten arc-weld [12, 13].

A few hypotheses as to how to account for lacking physics, and thus improve the prediction of weld pool models, have been proposed and tested by other authors. One

*Corresponding author
Email address: A.Kidess@tudelft.nl (Anton Kidess)

Nomenclature

A	Aspect ratio	T_s, T_l	Solidus and liquidus temperature
c_p	Heat capacity	$\boldsymbol{u}$	Fluid velocity
$\frac{D}{Dt}$	Material derivative	U_c	Characteristic velocity
D_c	Characteristic length scale (pool depth)	$\overline{\boldsymbol{u}}$	Mean velocity
$\boldsymbol{F}_{damp}$	Momentum sink term due to solidification	u'	Velocity fluctuation
g	Volume fraction of solid	**Greek symbols**	
h_f	Latent heat of fusion	ϵ	Turbulent kinetic energy dissipation rate
k	Turbulent kinetic energy	η	Laser absorptivity
L_c	Characteristic length scale (pool radius)	γ	Surface tension
L_K	Kolmogorov length scale	λ	Thermal conductivity
P	Laser power	μ	Dynamic viscosity
p	Pressure	ν	Kinematic viscosity
r_q	Laser beam radius	ω	Vorticity
S_{latent}	Latent heat source term	ρ	Density
T	Temperature	**Subscripts**	
t	Time	n	Normal direction
t_K	Kolmogorov time scale	t	Tangential direction

identified deficiency is the common comparison of post-solidification weld pool shapes with numerical simulation results not including the solidification stage. Ehlen et al. [14] and Saldi et al. [15] have determined that the weld pool shape can significantly change during this last stage of a welding process. Unfortunately, while the inclusion of the solidification stage can improve the predictions in some situations, it still does not ensure predictive capabilities [15].

Another possible source of error may be attributed to the often neglected motion of the liquid-gas interface. Simulations conducted by Ha and Kim [16] based on Pitscheneder's laser welding experiments [7] however show a very limited influence of a deformable free surface on the weld pool shape. The same conclusion has been made by Zehr [11] based on 3D simulations of conduction-mode laser welding.

Winkler et al. [1] have proposed the lack of surface chemistry and surface mass transfer processes in published models, resulting in a homogeneous distribution of surface active elements such as sulfur in the pool and at its surface, as potential source of the discrepancy. The group was able to improve their predictions using a mass transport model for a surface active element [17], and even more so when taking into account the effect of multiple surfactants [18][1]. However, even though their results using a laminar flow assumption are promising, they do conclude that there is a need to address the question of turbulent flow in weld pools. This conclusion is reinforced by the previously mentioned experimental observations of flow instabilities which are not seen in the simulations by Winkler et al. even when including the effects of surfactant redistribution.

Although sometimes done without explicit justification (e.g. He et al. [20], Roy et al. [21]), the hypothesized occurrence of turbulence has been a natural reasoning for many authors (e.g. Anderson et al. [3], Choo and Szekely [22]) to justify increasing transport coefficients, which given turbulent flow would occur naturally due to turbulent diffusion. A few authors have attempted to replace the tuning of

[1] It should be noted that Winkler et al. use a value for the standard heat of absorption in disagreement with the commonly used value [19], which may have lead to fortuitous improvement of the results due to a resulting altered surface tension temperature dependency $d\gamma/dT$.

transport properties by the use of turbulence models such as RANS [23–36] or LES [37]. While this leads to improved agreement with experiments (as does any increase of transport coefficients), the use of particularly RANS turbulence models developed for aerodynamics in complexly shaped, Marangoni driven weld pool flows with a free surface and non-smooth solid-liquid interface, is questionable. In fact, Pavlyk and Dilthey [2] conclude their numerical study of a gas-tungsten-arc weld with the statement "that neither an increase of the transport coefficients by a constant factor nor an application of the k-ϵ model improved the correspondence between the predicted and actual weld pool shapes", and support further investigation of the role of turbulence in such flows.

To analyze the possible role of turbulence, Chakraborty and Chakraborty [38] have presented a scaling analysis for high energy surface melting processes such as the laser welding process of interest here. The analysis allows the estimation of the flow regime based on three dimensionless numbers: *(i)* the melt pool depth-to-radius aspect ratio $A = D/L$, *(ii)* the Prandtl number Pr and *(iii)* a dimensionless number N inversely proportional to the Marangoni number Ma, $N = \left(\mu \,/(\rho \left|\partial\gamma/\partial T\right| \eta P/(\mu\pi\lambda))\right)^{1/3}$.

For the Pitscheneder experiment (see table 1 for material properties) at a welding power of 5200 W and a sulfur concentration of 150 ppm, the values of those dimensionless numbers are $A \approx 1.5$, $Pr = 0.178$ and $N \approx 0.01$. According to the analysis by Chakraborty and Chakraborty [38], the onset of turbulence is expected for $2A^{2/3}N^{-2} \geq \mathcal{O}(Re_{crit})$, where Re_{crit} is estimated from experiments to be around 600 [38, 39]. Turbulent thermal diffusion is predicted to exceed molecular thermal diffusion when $Pr \geq \mathcal{O}(25N^2A^{-2/3})$. Here, $2A^{2/3}N^{-2} \simeq 2.6 \cdot 10^4$, and $25N^2A^{-2/3} \simeq 2 \cdot 10^{-3}$, indicating the flow to be turbulent.

Now that we have established a need to investigate the possibility of turbulent flow and heat transport in melt pools, we will use simulations with very high temporal and spatial resolution to investigate the significance of turbulence without having to resort to questionable modelling techniques. To date, no such simulation results of welding have been published, as even with access to supercomputing facilities the computational cost remains substantial for long welding times. The stationary conduction-mode laser welding experiments by Pitscheneder et al. [7] will be used as an attractive test case for the hypothesis of the occurrence of turbulence, as uncertainties in boundary conditions are minimized while still exhibiting the need for significantly enhanced transport coefficients in laminar simulations in order to match the experimental results. In our simulations, we assume a uniform surfactant distribution in the weld pool, thus focusing on thermal Marangoni effects as a cause for turbulent flow instabilities. Non-uniform surfactant distributions will most likely further contribute to flow instabilities. As such, our present study may be considered as a "best case scenario" for the occurrence of turbulent flow instabilities.

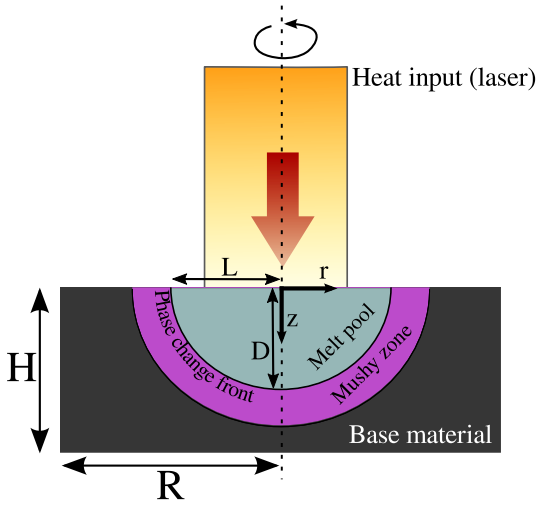

Figure 1: Schematic representation of the studied laser welding.

2. Model formulation

2.1. Governing equations

A schematic of a typical weld is shown in figure 1, where a slab of metal is targeted by a high power laser, where the relative speed between the laser and the target is zero. The laser irradiation will be absorbed by the target material, leading to an increase in temperature and eventually a melting phase change. Heat will be transferred into the bulk of the welded material by conduction and thermocapillary driven convection. These phenomena are mathematically modeled with an energy transport equation with a source term for the latent heat of the phase change

$$\frac{D}{Dt}(\rho c_p T) = \nabla \cdot (\lambda \nabla T) + S_{latent} \tag{1}$$

Due to the non-uniform heating of the top surface, large temperature gradients will develop. These temperature gradients result in gradients in surface tension, leading to thermocapillary forces along the non-deformable liquid-gas interface driving flow in the melt pool. The momentum transport is described by the Navier-Stokes equations, with a momentum sink that models the friction in the so-called mushy zone, where the liquid and solid phase co-exist

$$\frac{D}{Dt}\boldsymbol{u} = -\frac{1}{\rho}\nabla p + \nabla \cdot (\nu \nabla \boldsymbol{u}) - \boldsymbol{F}_{damp} \tag{2}$$

Here, we have assumed constant density over all phases.

2.1.1. Latent heat release

The effect of melting and solidification on the heat transfer are taken into account via the source term S_{latent} in equation 1

$$S_{latent} = \rho h_f \frac{dg}{dt} \tag{3}$$

with g the volume fraction of solid material, which is assumed to vary linearly over the melting temperature range between solidus and liquidus

$$g = \frac{T_l - T}{T_l - T_s},\ T_s < T < T_l \tag{4}$$

2.1.2. Coupling of momentum and heat transport

Through the inclusion of the momentum sink term, the momentum equation 2 is valid for the entire domain including both liquid and solid regions. The (semi-)solid regions are modeled as a porous medium, introducing a momentum sink following the isotropic Blake-Kozeny model [40]

$$\boldsymbol{F}_{damp} = \frac{\mu}{K\rho}\boldsymbol{u} \tag{5}$$

$$K = K_0 \frac{g^2}{(1-g)^3 + \varepsilon} \tag{6}$$

with $\mu/K_0 = 10^6\,\mathrm{N\,s\,m^{-4}}$ and $\varepsilon = 10^{-3}$. A similar approach has successfully been applied in DNS by Breugem et al. [41].

2.2. Boundary conditions

For 2D simulations we assume the melt pool to be axisymmetrical and make use of this by only simulating a wedge of the domain. Circumferential gradients are zero on the wedge faces. The conditions on the remaining boundaries (which are the same in 2D and 3D) are outlined in the following.

2.2.1. Heat input

At the top surface, the laser irradiation is modeled by a top-hat distributed heat flux. Because the heat loss due to radiation and convection is only a small fraction of the laser irradiation, we apply adiabatic boundary conditions everywhere except the irradiated area, where we apply a top-hat distribution as

$$\lambda \nabla_n T\Big|_{z=0} = \frac{\eta P}{\pi r_q^2},\ r \leq r_q \tag{7}$$

Here we follow Pitscheneder et al. [7] with $\eta = 0.13$, $P = 5200\,\mathrm{W}$ and $r_q = 1.4\,\mathrm{mm}$.

2.2.2. Momentum

At the liquid-gas interface, we introduce a shear stress in the liquid due to surface tension gradients along the interface (Marangoni force):

$$\mu \nabla_n u_t\Big|_{z=0} = \frac{d\gamma}{dT}\nabla_t T \tag{8}$$

The variation of surface tension with temperature is computed using the thermochemical model of Sahoo et al. [19]. The relevant curve for a sulfur concentration of 150 ppm is plotted in figure 2. Experimentally, such a behaviour with a sign change at a critical temperature has been shown to occur in steels [42, 43] and pure iron [44], as well as other metals such as silver [44] and nickel [45].

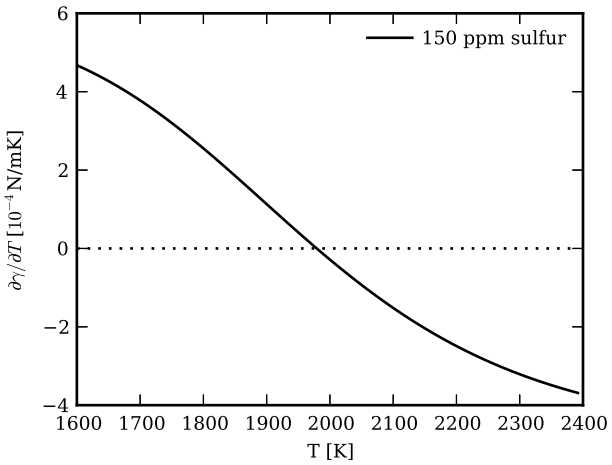

Figure 2: Surface tension temperature coefficient

Based on the small Capillary number $Ca = \mathcal{O}(10^{-2})$ for the studied weld pool, indicating that surface tension will effectively counter-act deformations due to fluid flow, we assume the free surface to be non-deformable. This assumption is in line with the observations by Ha and Kim [16], who investigated the influence of free surface deformations for the Pitscheneder et al. [7] case and concluded it is not important. The non-deformable surface assumption, however, may not hold for other welding processes and conditions at higher Capillary numbers, as experimental results show [12, 13, 46].

At all other surfaces, we set the velocity to zero.

3. Numerical procedure

Our solver is built on top of the open source finite volume framework OpenFOAM (version 2.1.x) [47].

We use a 2nd order backward differencing time marching scheme, and a 2nd order TVD scheme (limitedLinear [48]) for the divergence terms. At every time step, the non-linearity associated with the pressure-velocity-coupling is handled by the iterative PISO algorithm [49]. Once a divergence free velocity field has been computed at a given time step, the energy transport equation (1) is solved. If a phase change occurs, the temperature equation will be non-linear. The non-linearity due to latent heat is dealt with using an implicit source term linearization technique [50].[2]

To properly resolve the turbulent structures in space and time using direct numerical simulations, we estimate the length and time scales of the smallest turbulent eddies (Kolmogorov scales), which depend on a characteristic velocity and a characteristic length scale. Looking at

[2]The solver and input files will be made available through the journal's supplementary material.

Table 1: Material properties of the S705 alloy [7]

Property	Value	Unit
Solidus temperature T_s	1610	K
Liquidus temperature T_l	1620	K
Specific heat capacity c_p	670	$\mathrm{J\,kg^{-1}\,K^{-1}}$
Density ρ	8100	$\mathrm{kg\,m^{-3}}$
Thermal conductivity λ	22.9	$\mathrm{W\,m^{-1}\,K^{-1}}$
Latent heat of fusion h_f	$2.508 \cdot 10^5$	$\mathrm{J\,kg^{-1}}$
Viscosity μ	$6 \cdot 10^{-3}$	Pa s
Surface tension temperature coefficient $\partial\gamma/\partial T\|_0$	$-5.0 \cdot 10^{-4}$	$\mathrm{N\,m^{-1}\,K^{-1}}$
Entropy factor	$3.18 \cdot 10^{-3}$	–
Standard heat of adsorption	$-1.66 \cdot 10^8$	$\mathrm{J\,kmol^{-1}}$
Surface excess at saturation	$1.3 \cdot 10^{-8}$	$\mathrm{kmol\,m^{-2}}$

the experimental and numerical results reported by Pitscheneder et al. [7], we estimate a characteristic velocity $U_c \approx 0.2\,\mathrm{m\,s^{-1}}$, and a characteristic length scale of $2L_c \approx 4 \times 10^{-3}$ m. Now with the turbulent kinetic energy dissipation rate $\epsilon \approx U_c^3/D$, the Kolmogorov length scale is estimated by

$$L_K = \left(\frac{\nu^3}{\epsilon}\right)^{1/4} = \left(\frac{D\nu^3}{U_c^3}\right)^{1/4} \approx 2 \times 10^{-5}\,\mathrm{m} \qquad (9)$$

The Kolmogorov time scale is given by

$$t_K = \left(\frac{\nu}{\epsilon}\right)^{1/2} \approx 6 \times 10^{-4}\,\mathrm{s} \qquad (10)$$

The solution domain is a cylinder of radius $R = 7.5$ mm and height $H = 7.5$ mm, discretized with a mesh of 4.8 million cubic control volumes. The area where we expect fluid flow consists of small cubes with a a cell spacing of 23 µm, whereas we use larger cells of 188 µm away from the liquid region. The mesh is shown in figure 3. The time step is dynamically set obeying a maximum Courant number of $Co = U\Delta t/\Delta x < 0.33$, resulting in a typical time step of less than 1×10^{-5} s.

To further demonstrate the sufficient resolution of our mesh for proper direct numerical simulation (DNS) of the liquid, anticipating the simulation results presented in the next section, we determine the distribution of the turbulence dissipation rate in the simulated flow as $\epsilon = \nu\overline{\nabla \boldsymbol{u}' : \nabla \boldsymbol{u}'}$, with the computed velocity fluctuations $\boldsymbol{u}' = \boldsymbol{u} - \overline{\boldsymbol{u}}$. The ratio of the mesh spacing Δx and the smallest turbulence length scales L_K, based on the simulated velocity and dissipation averaged over a time of 0.5 s, is plotted in figure 4 for a slice through the pool, showing excellent resolution of even the smallest scales in our simulations. Only a very small region near the stagnation point at the surface, consisting of few mesh cells, is under-resolved by a factor up to 4.

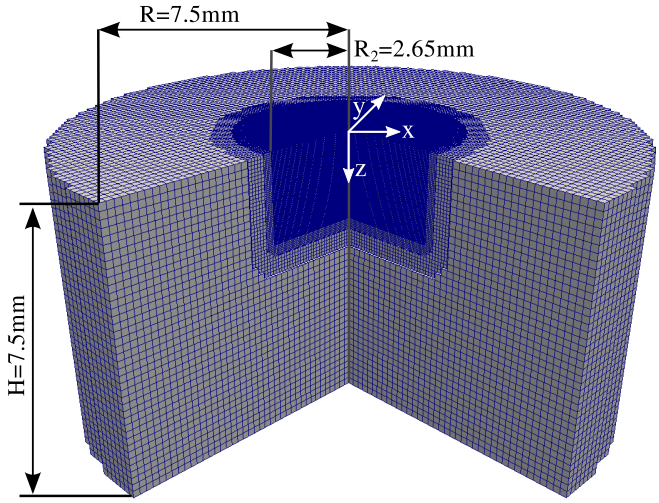

Figure 3: 3D mesh, where one quarter of the domain has been clipped for visualization. The coarse outer mesh with a grid cell size of 188 µm is refined in three steps to the finest inner mesh with a grid cell size of 23 µm. The latter is too fine to be resolved in this figure.

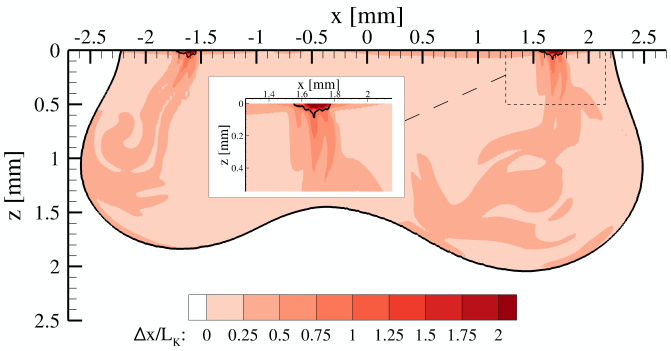

Figure 4: Grid size to turbulent length scale ratio $\Delta x/L_K$ in the in the y=0 mm plane, with the dissipation ϵ averaged over a time of 0.5 seconds. A length scale ratio smaller than 1 means turbulence is perfectly resolved, which is the case everywhere except a small region near the stagnation point at the surface (separated by a black line, with a maximum value of 4). This and subsequent figures show (quasi) instantaneous cross sections of the strongly unstable and non-axisymmetric weld pool. Such cross sectional snapshots are therefore presented in the x-z plane at y=0 of a Cartesian coordinate system, rather than the r-z coordinate system used in figures 1-3.

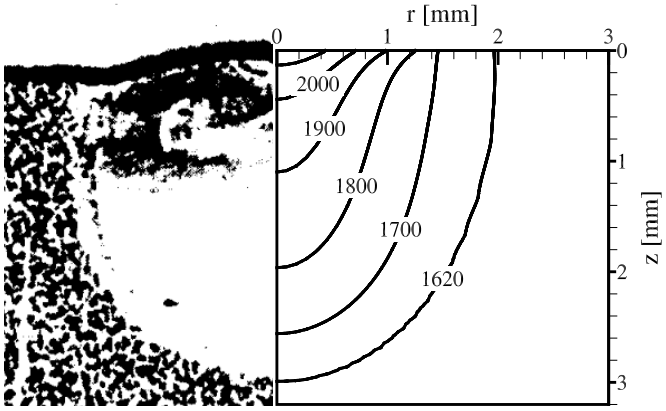

Figure 5: The right hand side of the figure shows the current faithful representation of the experimental result (left half of the figure, reproduced from [7] with permission of the publisher, sized to match scale on the right) after 5 s of welding, using an enhancement factor of 7 for both the viscosity and the thermal conductivity. Temperature isolines in Kelvin (simulation result, right half).

4. Results and Discussion

4.1. Verification with enhanced transport coefficients

In order to obtain good agreement between their numerically simulated melt pool shapes and experimentally observed post-solidification weld shapes, Pitscheneder et al. [7] artificially enhance the viscosity and thermal conductivity of the welded steel by a non-elucidated constant factor 7. We can reproduce their result using this constant enhancement factor, when, as done by Pitscheneder et al., we use a coarse 2D-axisymmetric grid[3], relatively large time steps, and a diffusive upwind discretization scheme (see figure 5). Without artificially increasing the transport coefficients, i.e. when using physically realistic values for the viscosity and the thermal conductivity, the flow within the melt pool differs significantly and so does the obtained final weld pool shape, as we will show in the following section.

4.2. Direct numerical simulations without enhancement of transport properties

The melt pool shape after 5.00 s of heat input, obtained from three-dimensional direct numerical simulations with realistic (non-enhanced) transport properties, is shown in figure 6. Also shown are melt pool shape snapshots after 4.27 s and 4.70 s of heat input. Compared to the results obtained with enhanced transport coefficients and a diffusive numerical scheme on a coarse 2D mesh, as shown in figure 5, it is now clearly visible that *(i)* the flow has not remained symmetric, leading to an asymmetric melt pool shape at this time instance; *(ii)* the melt pool is a bit wider and much less deep, leading to a pool depth-to-radius aspect ratio which is now smaller than 1; *(iii)* The melt pool shape is now strongly time dependent and oscillating.

These observations may be understood as follows: Due to the low (i.e. non-enhanced) molecular thermal conductivity, higher temperatures are now sustained at the melt pool surface, which lead to a large region subject to a negative surface tension gradient, in place of the previously dominant positive surface tension gradient (figure 2). The latter caused a flow directed inward along the pool surface, and towards the pool bottom along its axis, resulting in a deep, hemispherical pool shape as shown in figure 5. The sign change in the surface tension gradient now leads to a surface flow directed radially outward from the pool centre, rather than the inward directed flow in the 2D simulation with enhanced transport coefficients. This results in a wide, shallow pool, rather than a deep, narrow pool. At the edge of the melt pool surface, where temperatures are lower, the surface tension gradient is still positive. As a result, the radially outward surface flow from the pool centre impinges onto a second surface flow directed radially inward from the edge of the pool towards the pool centre. At the point where the two opposing flows meet, at a radial distance of roughly 1.5 mm, a circular, downward jet from the pool surface towards the base of the pool is formed. The downward jet is unstable, as both its origin and its angle oscillate in time. We use the term "instability" as it stresses that the initially laminar flow has transitioned into a chaotic state, and not a mere regular laminar unsteadiness. The general flow topology has been anticipated by Mills et al. [51] and Keene et al. [52]. Mills et al. also comment on the possibility of thermocapillary instabilities arising due to temperature gradients normal to the free surface, based on a theory formulated by Nemchinsky [53] assuming constant $\partial\gamma/\partial T$. Here however, in contrast to the case of Nemchinsky, the downward jet is clearly the dominating source of turbulent motion, as opposed to capillary waves at the free surface. The oscillating downward jet due to the sign change in surface tension also sets the present case apart from previous investigations of thermocapillary instabilities with constant, negative $\partial\gamma/\partial T$ [54–57].

The oscillating, hot, downwardly directed jet transports so much heat away from the surface that the melt pool boundary is continuously melting and re-solidifying, depending on where the jet is facing at a given time instance. This causes the oscillation of the pool boundary, as visible from the overlayed pool shapes at two additional time instances in figure 6. The flow is also strongly three dimensional, with significant, unsteady flow present in the azimuthal direction (figure 7). The flow pattern and vorticity ω at various time instances around $t = 3.0$ s, roughly 0.01 s apart, is shown in figure 8. During these time instances the right jet oscillates back and forth, whereas the left jet is relatively stable. This is of course not true for all time instances, highlighting the chaotic nature of the independent motion of the two jets.

[3]Strongly refined towards the free surface and pool centre, with the smallest $\Delta r = 90\,\mu$m and $\Delta z = 12\,\mu$m

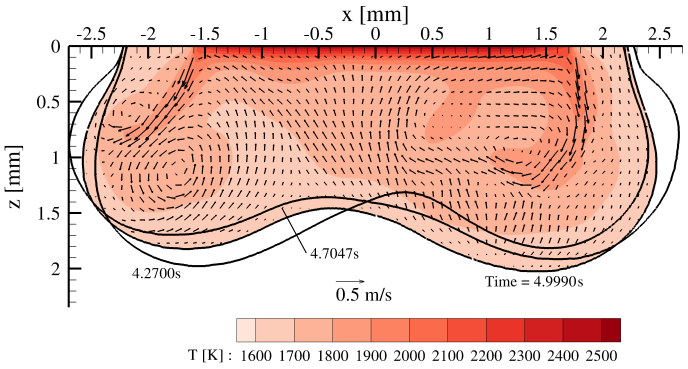

Figure 6: Melt pool shape, temperatures (in Kelvin) and velocity vectors in the y=0 mm plane at the end of heating $t = 5.0\,\mathrm{s}$. Note that the velocity vectors have been interpolated to a coarse grid in post-processing for clarity. The pool shape at two other time instances is overlayed, showing the pool boundary oscillation.

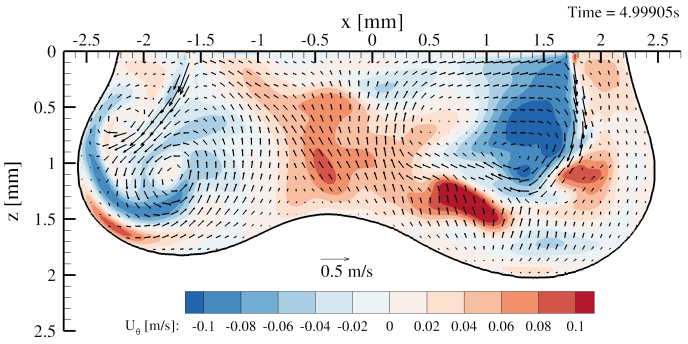

Figure 7: In-plane (x,z) velocities in the y=0 mm plane at $t = 5.0\,\mathrm{s}$ indicated by vectors, and out-of-plane (azimuthal) velocities indicated by colour contours.

The melt pool flow instabilities are also visible in the temperatures at the pool surface, shown in figure 9. The oscillations are most apparent in the centre of the pool where the oscillation frequency is high, but also at the rim of the pool with a lower frequency due to the dampening effect of melting and re-solidification.

At the stagnation line, where the radially outward surface flow from the pool centre impinges on the radially inward surface flow from the pool edge and where there is a sign change in the surface tension coefficient, very high thermal gradients of $\mathrm{O}(3000\,\mathrm{K\,mm^{-1}})$ occur. Since the thermocapillary force is proportional to these thermal gradients, this is also where we encounter the highest flow velocities (figure 10), locally as high as $2\,\mathrm{m\,s^{-1}}$.

4.3. Analysis of turbulent flow properties

We now address a more quantitative analysis of the turbulent nature of the melt pool flow, and the importance of turbulent heat transfer.

Using the computed instantaneous velocity fluctuations $\boldsymbol{u}' = \boldsymbol{u} - \bar{\boldsymbol{u}}$, we can determine the turbulent kinetic energy $k = \overline{\boldsymbol{u}' \cdot \boldsymbol{u}'}/2$, and the turbulent viscosity as $\nu_t = 0.09k^2/\epsilon$, with the turbulent kinetic energy dissipation rate $\epsilon = \nu\overline{\nabla\boldsymbol{u}' : \nabla\boldsymbol{u}'}$. Here, all averages have been computed over the time interval between 4.5 and 5s. The results are shown in figures 11 and 12, respectively. The turbulent kinetic energy takes its highest values near the extreme positions of the jet and near the stagnation point at the free surface. The turbulent viscosity assumes its largest values of roughly 50 times the molecular value in an area around the end point of the jet. The space averaged value of the turbulent viscosity is approximately 7.4 times the molecular value. This, coincidentally, is close to the factor 7 enhancement for the transport properties used by Pitscheneder et al. [7] to match their experimental results. However, the uniform enhancement used by Pitscheneder et al. leads to distinctly different melt pool shapes than the turbulent enhancement following from our DNS simulations. In the first, a hemispherical melt pool shape is obtained which is deepest at the centre, whereas the maximum turbulent enhancement occurs in the oscillating jet regions and causes the pool to be wider and deeper at the edges.

To further quantitatively investigate the oscillating flow, we track a monitoring point at a distance of x=1 mm and a depth of z=1 mm from the centre of the pool surface. The temperature history at this monitoring point is shown in figure 13a. After reaching a quasi steady state, it shows an irregular oscillation with an amplitude of about 200 K around a mean temperature of 1720 K. The velocity magnitude at the monitoring point (figure 13b) oscillates violently with an amplitudes of roughly 50% of its mean value.

The frequency spectrum of the temperature and velocity magnitude signals at the monitoring point, obtained by a discrete Fourier transform (DFT) of the signals for

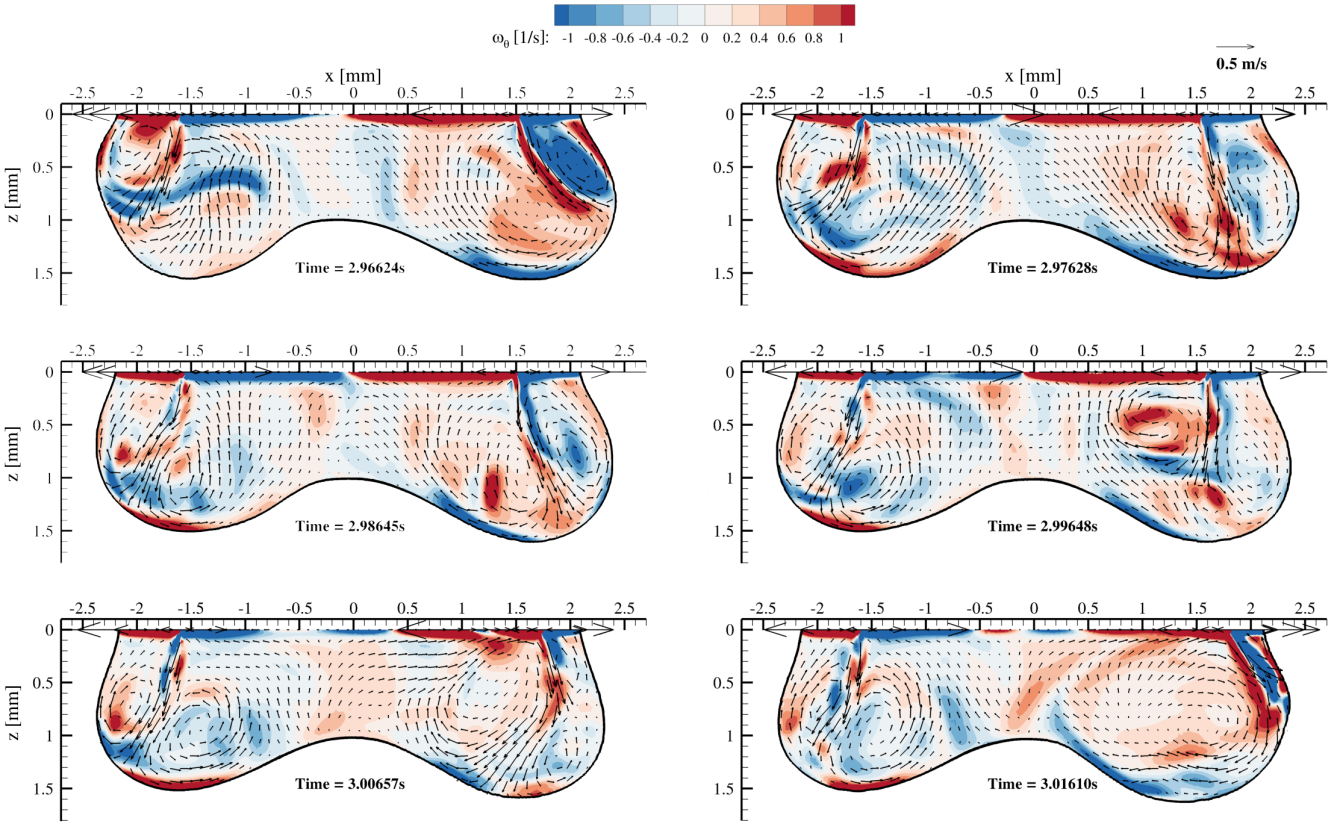

Figure 8: In-plane (x,z) velocity vectors in the y=0 mm plane at a few time instances around $t = 3.0$ s (approximately 0.01 s apart), and out-of-plane vorticity contours.

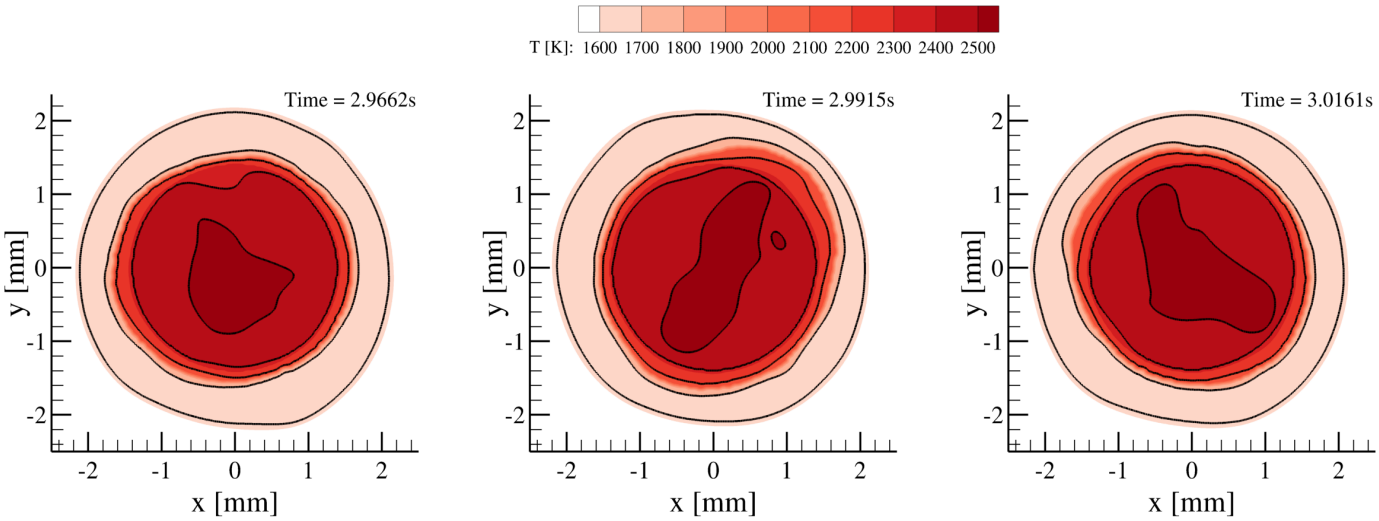

Figure 9: Pool surface (z=0 mm) temperatures in Kelvin at three time instances, top view. Isolines are drawn at 1620K, 1700K, 2200K, 2400K and 2500K (from outside to inside).

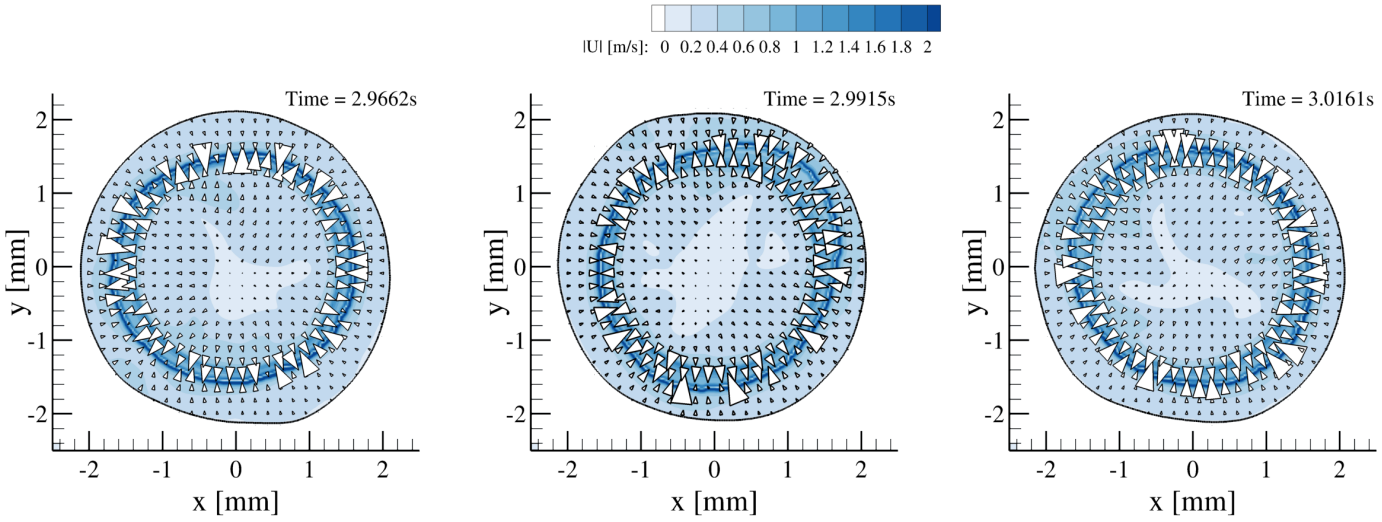

Figure 10: Pool surface (z=0 mm) flow at three time instances, top view. The largest vectors in the vicinity of the stagnation point have been blanked for clarity.

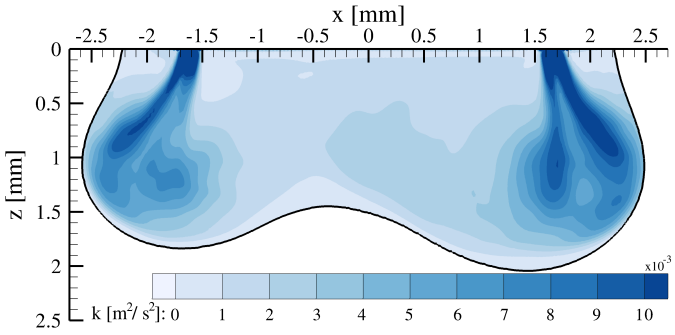

Figure 11: Turbulent kinetic energy k in the y=0 mm plane, averaged over 0.5 s.

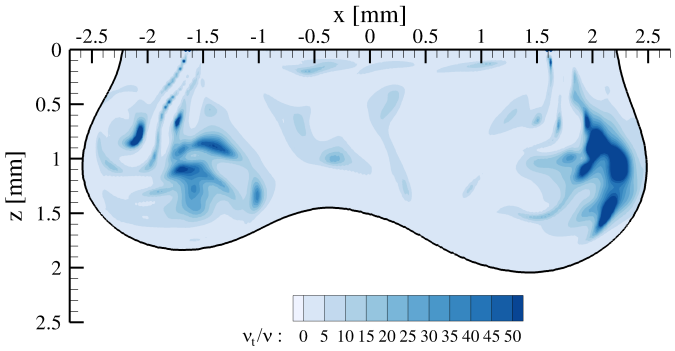

Figure 12: Ratio of turbulent diffusivity over molecular diffusivity ν_t/ν in the y=0 mm plane, based on turbulent kinetic energy and turbulence dissipation averaged over 0.5 s.

the quasi steady state period between 2 and 5 seconds after the onset of heating, is shown in figures 14a and 14b, respectively. Both spectra exhibit multiple peaks in the low-frequency region up to 10 Hz. Due to the low Prandtl number of the fluid, momentum diffusivity is small compared to thermal diffusivity. As a result, high frequency oscillations are more strongly damped for temperature as compared to velocity. The temperature signal drops beyond 10 Hz, whereas the velocity signal only starts dropping around 30 Hz. The most dominant frequencies in the temperature spectrum are around 5, 7 and 11 Hertz, which also appear in the spectrum of the velocity magnitude, though accompanied here by many other peaks up to 30 Hertz.

4.4. The 3D nature of the flow instabilities

To unravel to which extent the complexity and oscillating instability of the melt pool flow is related to its three-dimensionality, we have also performed a high-fidelity two-dimensional axisymmetric simulation with a mesh that was very similar to that of the 3D simulations, and identical numerical schemes. The 2D simulated flow, unlike earlier published 2D flow simulations with enhanced transport coefficients on coarse meshes with diffusive numerical schemes, exhibits a highly unstable nature, very similar to that observed in the 3D simulations. A characteristic flow oscillation is shown in figure 15. The, now axisymmetric, circular downward jet stemming from the stagnation point at the free surface shows qualitatively the same oscillatory pattern as observed in the 3D simulations. It may therefore be concluded that the additional degree of freedom

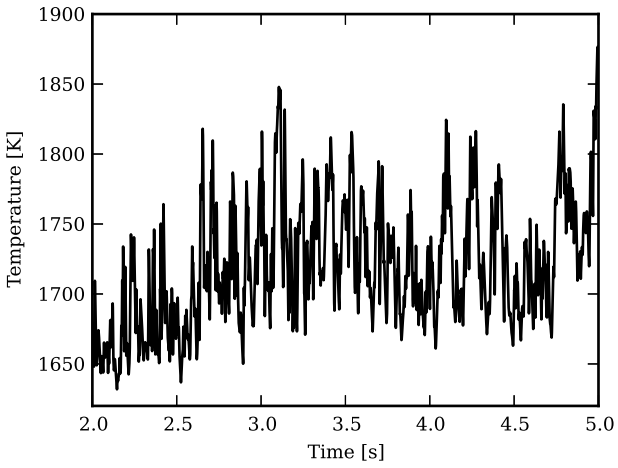

(a) Temperature at monitoring point.

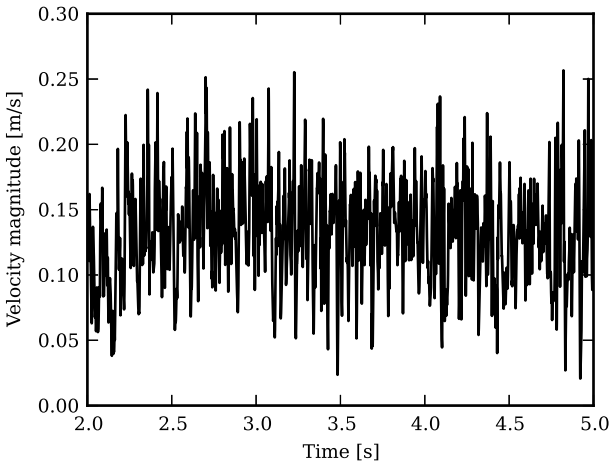

(b) Total velocity magnitude at monitoring point.

Figure 13: Temperature and velocity magnitude at monitoring location x=1 mm, y=0 mm, z=1 mm

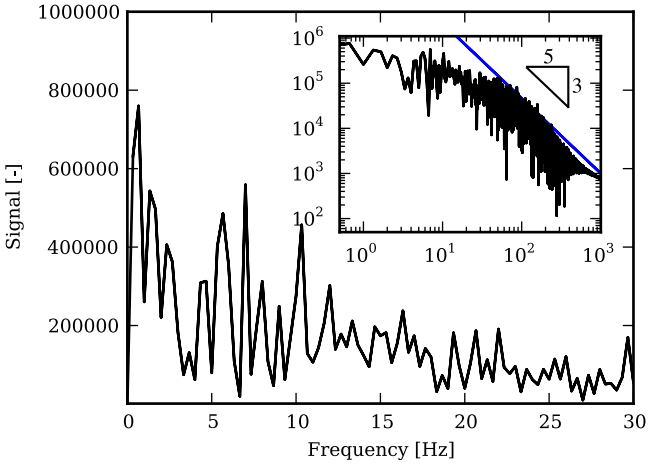

(a) DFT of temperature at monitoring point

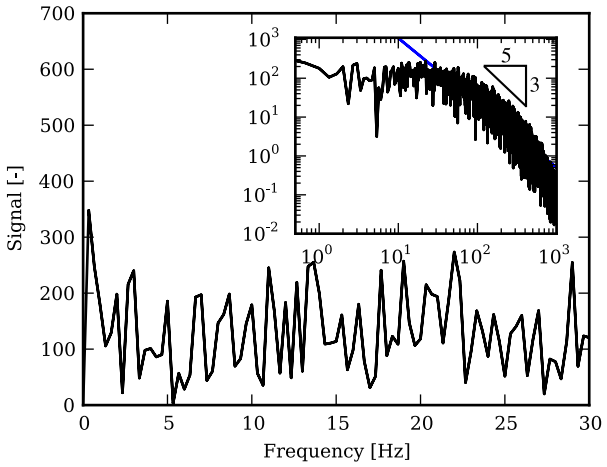

(b) DFT of velocity magnitude at monitoring point

Figure 14: DFT of temperature and velocity magnitude at monitoring point x=1 mm, y=0 mm, z=1 mm. Inserts on log-log scale, in which, as a reference, a blue line with -5/3 slope is shown.

of three-dimensionality is not a requirement for triggering the jet instability. However, in the 2D case the oscillation is much more regular, which can easily be observed from in the temperature signal at the monitoring point (figure 15). While the amplitude of the oscillation of roughly 250 K is even larger than in the 3D flow, the oscillation frequency is low and regular, with large peaks in the spectrum reoccurring at roughly 4 Hz.

A similar oscillation pattern has been reported in literature for the case of a slot jet impinging on a concave curved wall [58]. However, in the presently studied melt pool flow, at least in 2D, the instability appears not to be simply due to the interaction between the impinging jet and the concave bottom of the pool, but stems from a more complex interplay between the jet, its oscillating origin, and the constantly deforming melt pool bottom due to melting and re-solidification. We performed a 2D axisymmetric simulation in which, after a quasi steady-state with strong jet oscillations had been reached, further melting (and re-solidification) of the pool boundary was prevented by artificially increasing the latent heat of melting by a factor 100, thus de facto fixing the pool boundary. With this fixed pool boundary, the jet oscillations quickly died out and the flow became steady-state. This demonstrates that, at least in 2D, the interplay with a deforming melt pool boundary is necessary to sustain the jet oscillations. The same fixation of the pool boundary in 3D did not lead to a suppression of the oscillations, indicating that the 3D case is more prone to instabilities than the 2D case.

5. Conclusion and outlook

We have simulated the liquid metal flow in the melt pool of a conduction-mode laser weld, using high-fidelity direct numerical simulations to gain insight into flow instabilities that have been reported in experimental studies, but not in numerical studies to date.

In our simulations, unlike earlier numerical studies of weld pool flows that used coarse meshes, diffusive numerical schemes and enhanced transport coefficients, we observe self-sustained flow instabilities. These arise even in the absence of a deformable liquid-gas surface, temperature dependent material properties, or non-uniform surfactant concentrations. The instabilities even occur when restricting the flow to axial symmetry, albeit the oscillation is much more regular in that case.

The amplitude and frequency spectrum of the temperature and velocity oscillations support the argument of enhanced heat and momentum transport due to turbulent flow in the melt pool. Averaged in space, the turbulent diffusivities are approximately seven times higher than their molecular values. This turbulent transport enhancement is of the same order of magnitude as ad-hoc enhancement factors commonly used in previous studies to obtain agreement between numerical weld pool simulations and experimentally observed weld pool shapes. However, the observed turbulent enhancement is strongly non-uniform, and highest in the regions of the oscillating jets near the rim of the weld pool. Therefore, unlike in simulations assuming uniform transport enhancement and unlike experimentally observed for this case, our simulations lead to W-shaped melt pools that are deepest near the rim of the pool. More generally though, W-shaped pools have been observed by many authors [2, 14, 17, 59–61].

Thus, while we have clearly demonstrated the presence of turbulent flow instabilities and turbulent transport enhancement in laser weld pools, the predicted turbulence does not lead to proper melt pool shape predictions. We believe the most likely deficiency of our model to be in the assumed uniform surfactant concentration due to the lack of a mass transport model for surfactant species. Winkler et al. [17] have demonstrated that surfactant concentrations may actually be highly non-uniform, leading to strong alterations of the Marangoni forces and flow. The stagnating flow at the jet origin will lead to a local high concentration of surface active element [18], strengthening the local surface tension maximum and thus amplifying the Marangoni forces and the resulting flow. Hence, combining the results from Winkler et al. [17] with the present results, direct numerical or dynamic large eddy turbulence simulations coupled with a mass transport model for the surfactants are probably needed to move forward towards really predictive melt pool models for welding.

Acknowledgments

We would like to thank the European Commission for funding the MINTWELD project (reference 229108) via the FP7-NMP program. We thank SURFsara for the support in using the Lisa Compute Cluster (project MP-235-12).

References

[1] C. Winkler, G. Amberg, H. Inoue, T. Koseki, A numerical and experimental investigation of qualitatively different weld pool shapes, in: H. Cerjak, H. K. D. H. Bhadeshia (Eds.), Mathematical Modelling of Weld Phenomena 4, Materials Modelling Series, IOM Communications Ltd, London, ISBN 1-86125-060-6, 37–69, 1997.

[2] V. Pavlyk, U. Dilthey, A numerical and experimental study of fluid flow and heat transfer in stationary GTA weld pools, in: H. Cerjak, H. K. D. H. Bhadeshia (Eds.), Mathematical Modelling of Weld Phenomena 5, Materials Modelling Series, IOM Communications Ltd, ISBN 1 86125 115 7, 135–163, 2001.

[3] T. D. Anderson, J. N. DuPont, T. DebRoy, Origin of stray grain formation in single-crystal superalloy weld pools from heat transfer and fluid flow modeling, Acta Materialia 58 (4) (2010) 1441–1454, ISSN 13596454, doi:10.1016/j.actamat.2009.10.051.

[4] A. De, T. DebRoy, Probing unknown welding parameters from convective heat transfer calculation and multivariable optimization, Journal of Physics D: Applied Physics 37 (1) (2003) 140+, ISSN 0022-3727, doi:10.1088/0022-3727/37/1/023.

[5] A. De, T. DebRoy, A smart model to estimate effective thermal conductivity and viscosity in the weld pool, Journal of Applied Physics 95 (9) (2004) 5230–5240, doi:10.1063/1.1695593.

[6] A. De, T. DebRoy, Improving reliability of heat and fluid flow calculation during conduction mode laser spot welding by

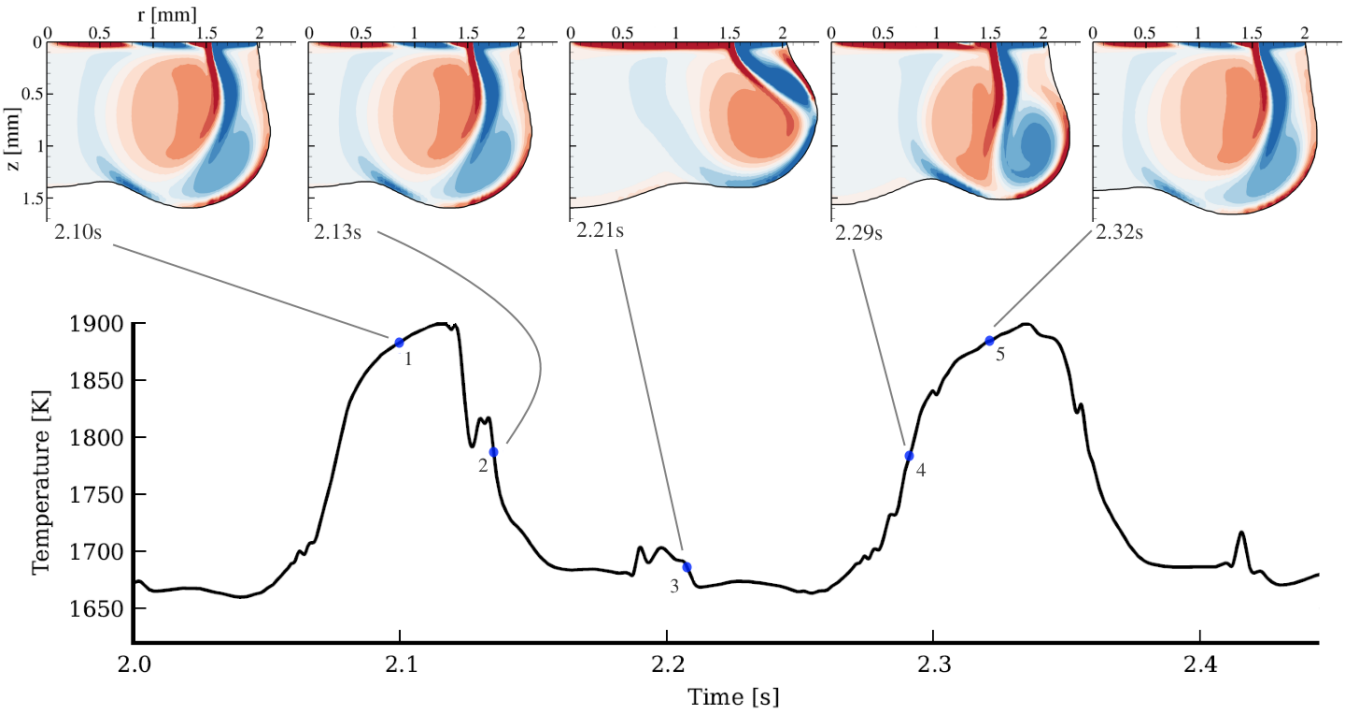

Figure 15: Two-dimensional flow vorticity at various time instances in the axisymmetric case, with corresponding temperature probe at a monitoring point at r=1mm, z=1mm

multivariable optimisation, Science and Technology of Welding and Joining 11 (2) (2006) 143–153, ISSN 1362-1718, doi: 10.1179/174329306x84346.

[7] W. Pitscheneder, T. DebRoy, K. Mundra, R. Ebner, Role of sulfur and processing variables on the temporal evolution of weld pool geometry during multikilowatt laser beam welding of steels, Welding Journal 75 (3) (1996) 71–s–80–s.

[8] W. Tan, N. S. Bailey, Y. C. Shin, Numerical Modeling of Transport Phenomena and Dendritic Growth in Laser Spot Conduction Welding of 304 Stainless Steel, Journal of Manufacturing Science and Engineering 134 (4) (2012) 041010+, ISSN 10871357, doi:10.1115/1.4007101.

[9] S. Mishra, T. J. Lienert, M. Q. Johnson, T. DebRoy, An experimental and theoretical study of gas tungsten arc welding of stainless steel plates with different sulfur concentrations, Acta Materialia 56 (9) (2008) 2133–2146, ISSN 13596454, doi: 10.1016/j.actamat.2008.01.028.

[10] H. G. Kraus, Surface Temperature Measurements of GTA Weld Pools on Thin-Plate 304 Stainless Steel, Welding Journal 68 (3) (1989) 84–s–91–s.

[11] R. L. Zehr, Thermocapillary convection in laser melted pools during materials processing, Ph.D. thesis, University of Illinois at Urbana-Champaign, 1991.

[12] C. X. Zhao, V. van Steijn, I. M. Richardson, C. R. Kleijn, S. Kenjeres, Z. Saldi, Unsteady interfacial phenomena during inward weld pool flow with an active surface oxide, Science and Technology of Welding & Joining 14 (2) (2009) 132–140, ISSN 1362-1718, doi:10.1179/136217108x370281.

[13] C. Zhao, Measurements of fluid flow in weld pools, Ph.D. thesis, Delft University of Technology, 2011.

[14] G. Ehlen, A. Ludwig, P. R. Sahm, Simulation of time-dependent pool shape during laser spot welding: Transient effects, Metallurgical and Materials Transactions A 34 (12) (2003) 2947–2961, ISSN 1073-5623, doi:10.1007/s11661-003-0194-x.

[15] Z. S. Saldi, A. Kidess, S. Kenjereš, C. Zhao, I. M. Richardson, C. R. Kleijn, Effect of enhanced heat and mass transport and flow reversal during cool down on weld pool shapes in laser spot welding of steel, International Journal of Heat and Mass Transfer 66 (2013) 879–888, ISSN 00179310, doi: 10.1016/j.ijheatmasstransfer.2013.07.085.

[16] E.-J. Ha, W.-S. Kim, A study of low-power density laser welding process with evolution of free surface, International Journal of Heat and Fluid Flow 26 (4) (2005) 613–621, ISSN 0142727X, doi:10.1016/j.ijheatfluidflow.2005.03.009.

[17] C. Winkler, G. Amberg, H. Inoue, T. Koseki, M. Fuji, Effect of surfactant redistribution on weld pool shape during gas tungsten arc welding, Science and Technology of Welding and Joining 5 (1) (2000) 8–20, ISSN 1362-1718, doi: 10.1179/stw.2000.5.1.8.

[18] C. Winkler, G. Amberg, Multicomponent surfactant mass transfer in GTA-welding, Progress in Computational Fluid Dynamics, An International Journal 5 (3-5) (2005) 190–206, ISSN 1468-4349, doi:10.1504/pcfd.2005.006754.

[19] P. Sahoo, T. Debroy, M. McNallan, Surface tension of binary metal - surface active solute systems under conditions relevant to welding metallurgy, Metallurgical and Materials Transactions B 19 (3) (1988) 483–491–491, ISSN 0360-2141, doi: 10.1007/bf02657748.

[20] X. He, J. W. Elmer, T. DebRoy, Heat transfer and fluid flow in laser microwelding, Journal of Applied Physics 97 (8) (2005) 084909+, ISSN 0021-8979, doi:10.1063/1.1873032.

[21] G. G. Roy, J. W. Elmer, T. DebRoy, Mathematical modeling of heat transfer, fluid flow, and solidification during linear welding with a pulsed laser beam, Journal of Applied Physics 100 (3) (2006) 034903+, doi:10.1063/1.2214392.

[22] R. T. C. Choo, J. Szekely, The Possible Role of Turbulence in GTA Weld Pool Behaviour, Welding Journal 73 (2).

[23] N. Chakraborty, S. Chakraborty, P. Dutta, Modelling of turbulent transport in arc welding pools, International Journal of Numerical Methods for Heat & Fluid Flow 13 (1) (2003) 7–30, ISSN 0961-5539, doi:10.1108/09615530310456741.

[24] N. Chakraborty, D. Chatterjee, S. Chakraborty, Modeling of turbulent transport in laser surface alloying, Numerical Heat Transfer, Part A: Applications 46 (10) (2004) 1009–1032, doi: 10.1080/10407780490517629.

[25] N. Chakraborty, S. Chakraborty, Influences of Sign of Surface

Tension Coefficient on Turbulent Weld Pool Convection in a Gas Tungsten Arc Welding (GTAW) Process: A Comparative Study, Journal of Heat Transfer 127 (8) (2005) 848+, ISSN 00221481, doi:10.1115/1.1928913.

[26] N. Chakraborty, S. Chakraborty, P. Dutta, Three-dimensional modeling of turbulent weld pool convection in GTAW processes, Numerical Heat Transfer, Part A: Applications 45 (4) (2004) 391–413, doi:10.1080/10407780490250364.

[27] N. Chakraborty, S. Chakraborty, Modelling of turbulent molten pool convection in laser welding of a copper-nickel dissimilar couple, International Journal of Heat and Mass Transfer 50 (9-10) (2007) 1805–1822, ISSN 00179310, doi:10.1016/j.ijheatmasstransfer.2006.10.030.

[28] W. Dong, S. Lu, D. Li, Y. Li, GTAW liquid pool convections and the weld shape variations under helium gas shielding, International Journal of Heat and Mass Transfer 54 (7-8) (2011) 1420–1431, ISSN 00179310, doi:10.1016/j.ijheatmasstransfer.2010.07.069.

[29] M. Goodarzi, R. Choo, T. Takasu, J. M. Toguri, The effect of the cathode tip angle on the gas tungsten arc welding arc and weld pool: II. The mathematical model for the weld pool, Journal of Physics D: Applied Physics 31 (5) (1998) 569+, ISSN 0022-3727, doi:10.1088/0022-3727/31/5/014.

[30] K. Hong, D. Weckman, A. Strong, The influence of thermofluids phenomena in gas tungsten arc welds in high and low thermal conductivity metals, Canadian Metallurgical Quarterly 37 (3-4) (1998) 293–303, ISSN 00084433, doi:10.1016/s0008-4433(97)00021-9.

[31] K. Hong, D. C. Weckman, A. B. Strong, W. Zheng, Modelling turbulent thermofluid flow in stationary gas tungsten arc weld pools, Science and Technology of Welding and Joining (2002) 125–136ISSN 1362-1718, doi:10.1179/136217102225002619.

[32] K. Hong, D. C. Weckman, A. B. Strong, W. Zheng, Vorticity based turbulence model for thermofluids modelling of welds, Science and Technology of Welding and Joining (2003) 313–324ISSN 1362-1718, doi:10.1179/136217103225005507.

[33] J. Jaidi, K. S. S. Murthy, P. Dutta, A k-ϵ Model for Turbulent Weld Pool Convection in Gas Metal Arc Welding Process, in: S. A. David (Ed.), 6th International Trends in Welding Research Conference Proceedings, Trends in Welding Research, ASM International, ASM International, 147–152, 2002.

[34] J. Jaidi, P. Dutta, Three-dimensional turbulent weld pool convection in gas metal arc welding process, Science and Technology of Welding and Joining 9 (5) (2004) 407–414, ISSN 1362-1718, doi:10.1179/136217104225021814.

[35] A. K. Skouras, N. Chakraborty, S. Chakraborty, Computational Analysis of the Effects of Process Parameters on Molten Pool Transport in Cu-Ni Dissimilar Laser Weld Pool, Numerical Heat Transfer, Part A: Applications 58 (4) (2010) 272–294, doi:10.1080/10407782.2010.505154.

[36] X. Wang, D. Fan, J. Huang, Y. Huang, A unified model of coupled arc plasma and weld pool for double electrodes TIG welding, Journal of Physics D: Applied Physics 47 (27) (2014) 275202+, ISSN 0022-3727, doi:10.1088/0022-3727/47/27/275202.

[37] D. Chatterjee, S. Chakraborty, Large-eddy simulation of laser-induced surface-tension-driven flow, Metallurgical and Materials Transactions B 36 (6) (2005) 743–754, ISSN 1073-5615, doi:10.1007/s11663-005-0078-0.

[38] N. Chakraborty, S. Chakraborty, Thermal Transport Regimes and Generalized Regime Diagram for High Energy Surface Melting Processes, Metallurgical and Materials Transactions B 38 (1) (2007) 143–147, ISSN 1073-5615, doi:10.1007/s11663-006-9000-7.

[39] N. Chakraborty, Thermal Transport Regimes and Effects of Prandtl Number in Molten Pool Transport in Laser Surface Melting Processes, Numerical Heat Transfer, Part A: Applications 53 (3) (2007) 273–294, doi:10.1080/10407780701557709.

[40] A. Singh, R. Pardeshi, B. Basu, Modelling of convection during solidification of metal and alloys, Sadhana 26 (1) (2001) 139–162, ISSN 0256-2499, doi:10.1007/bf02728483.

[41] W. P. Breugem, B. J. Boersma, R. E. Uittenbogaard, The influence of wall permeability on turbulent channel flow, Journal of Fluid Mechanics 562 (2006) 35–72, ISSN 1469-7645, doi:10.1017/s0022112006000887.

[42] K. C. Mills, B. J. Keene, Factors affecting variable weld penetration, International Materials Reviews (1990) 185–216ISSN 0950-6608.

[43] S. Ozawa, K. Morohoshi, T. Hibiya, Influence of Oxygen Partial Pressure on Surface Tension of Molten Type 304 and 316 Stainless Steels Measured by Oscillating Droplet Method Using Electromagnetic Levitation, ISIJ International 54 (9) (2014) 2097–2103, ISSN 0915-1559, doi:10.2355/isijinternational.54.2097.

[44] T. Hibiya, S. Ozawa, Effect of oxygen partial pressure on the Marangoni flow of molten metals, Cryst. Res. Technol. 48 (4) (2013) 208–213, doi:10.1002/crat.201200514.

[45] S. Ozawa, S. Takahashi, N. Watanabe, H. Fukuyama, Influence of Oxygen Adsorption on Surface Tension of Molten Nickel Measured Under Reducing Gas Atmosphere 35 (9-10) (2014) 1705–1711, doi:10.1007/s10765-014-1674-5.

[46] S. Kou, C. Limmaneevichitr, P. Wei, Oscillatory Marangoni Flow: A Fundamental Study by Conduction-Mode Laser Spot Welding: Through Marangoni flow, a surface-active agent can affect not only the weld pool depth, but also the pool surface deformation, pool surface oscillation, and ripple formation, Welding Journal 90 (12).

[47] H. G. Weller, G. Tabor, H. Jasak, C. Fureby, A tensorial approach to computational continuum mechanics using object-oriented techniques, Computers in Physics 12 (6) (1998) 620–631, doi:10.1063/1.168744.

[48] E. Berberovic, Investigation of Free-surface Flow Associated with Drop Impact: Numerical Simulations and Theoretical Modeling, Ph.D. thesis, Technische Universitaet Darmstadt, 2010.

[49] R. I. Issa, Solution of the implicitly discretised fluid flow equations by operator-splitting, Journal of Computational Physics 62 (1) (1986) 40–65, ISSN 00219991, doi:10.1016/0021-9991(86)90099-9.

[50] V. R. Voller, C. R. Swaminathan, General source-based method for solidification phase change, Numerical Heat Transfer, Part B: Fundamentals: An International Journal of Computation and Methodology 19 (2) (1991) 175–189, doi:10.1080/10407799108944962.

[51] K. C. Mills, B. J. Keene, R. F. Brooks, A. Shirali, Marangoni effects in welding, Mathematical, Physical and Engineering Sciences 356 (1739) (1998) 911–925, ISSN 1471-2962, doi:10.1098/rsta.1998.0196.

[52] B. J. Keene, K. C. Mills, J. W. Bryant, E. D. Hondros, Effects of Interaction Between Surface Active Elements on the Surface Tension of Iron, Canadian Metallurgical Quarterly (1982) 393–403ISSN 0008-4433, doi:10.1179/000844382795243461.

[53] V. A. Nemchinsky, The role of thermocapillary instability in heat transfer in a liquid metal pool, International Journal of Heat and Mass Transfer 40 (4) (1997) 881–891, ISSN 00179310, doi:10.1016/0017-9310(96)00163-9.

[54] H. C. Kuhlmann, U. Schoisswohl, Flow instabilities in thermocapillary-buoyant liquid pools, Journal of Fluid Mechanics 644 (2010) 509–535, ISSN 1469-7645, doi:10.1017/s0022112009992953.

[55] C. Karcher, R. Schaller, T. Boeck, C. Metzner, A. Thess, Turbulent heat transfer in liquid iron during electron beam evaporation, International Journal of Heat and Mass Transfer 43 (10) (2000) 1759–1766, ISSN 00179310, doi:10.1016/s0017-9310(99)00248-3.

[56] T. Boeck, C. Karcher, Low-Prandtl-Number Marangoni Convection Driven by Localized Heating on the Free Surface: Results of Three-Dimensional Direct Simulations, in: R. Narayanan, D. Schwabe (Eds.), Interfacial Fluid Dynamics and Transport Processes, vol. 628 of *Lecture Notes in Physics*, Springer Berlin Heidelberg, 157–175, doi:10.1007/978-3-540-45095-5_8, 2003.

[57] B. Dikshit, G. R. Zende, M. S. Bhatia, B. M. Suri, Convec-

tion in molten pool created by a concentrated energy flux on a solid metal target, Physics of Fluids (1994-present) 21 (8) (2009) 084105+, ISSN 1070-6631, doi:10.1063/1.3210763.

[58] V. Gilard, L.-E. Brizzi, Slot Jet Impinging On A Concave Curved Wall, Journal of Fluids Engineering 127 (3) (2005) 595+, ISSN 00982202, doi:10.1115/1.1905643.

[59] D. K. Aidun, S. A. Martin, Effect of sulfur and oxygen on weld penetration of high-purity austenitic stainless steels, Journal of Materials Engineering and Performance 6 (4) (1997) 496–502, ISSN 1059-9495, doi:10.1007/s11665-997-0121-1.

[60] R. Daub, Erhöhung der Nahttiefe beim Laserstrahl-Wärmeleitungsschweißen von Stählen, Ph.D. thesis, Technische Universität München, 2012.

[61] M. Tanaka, Effects of surface active elements on weld pool formation using TIG arcs, Welding International 19 (11) (2005) 870–876, doi:10.1533/wint.2005.3517.